SPECIAL ISSUE - MINI REVIEW

Experimental tests of surface-enhanced Raman scattering: Moving beyond the electromagnetic enhancement theory

Sebastian Heeg | Niclas S. Mueller | Sören Wasserroth |

Patryk Kusch | Stephanie Reich

Department of Physics, Freie Universität Berlin, Berlin, Germany

Correspondence
Stephanie Reich, Department of Physics, Freie Universität Berlin, Arnimallee 14, 14195 Berlin, Germany.
Email: reich@physik.fu-berlin.de

Abstract

The electromagnetic enhancement theory describes surface-enhanced Raman scattering (SERS) as a Raman effect that takes place in the near-field of a plasmonic nanostructure. The theory has been very successful in explaining the fundamental properties of SERS, modelling the performance of different metals as enhancing materials and optimizing SERS hotspots for strongest possible enhancement. Over the last decade, a number of carefully designed experimental studies have examined predictions of the electromagnetic theory like the size and shape of SERS hotspots, the absolute magnitude of the enhancement and the width of the SERS resonance. Although the overall picture was quite satisfactory, the theory failed to predict key aspects of SERS, for example, the absolute magnitude of the plasmonic enhancement. We scrutinize these experiments and review them focusing on the results that require going beyond the electromagnetic enhancement theory. We argue that the results of these experiments create the need to develop the theory of SERS further, especially the exact role of plasmonic enhancement in inelastic light scattering.

KEYWORDS

absolute SERS enhancement, electromagnetic enhancement, plasmon, polarization, SERS

1 | INTRODUCTION

Surface-enhanced Raman scattering (SERS) overcomes the two main limitations of Raman scattering, its low sensitivity and limited spatial resolution.[1-3] Raman scattering evolved into a key experimental technique in the natural and life sciences. It allows the label-free detection of molecular species, following chemical reactions in real time, studying the interaction between quasi-particles in solids and characterizing materials for crystal quality, doping, strain and other fundamental parameters. The cross section of Raman scattering, however, is on the order of 10^{-22} to 10^{-24} cm^2 under resonant excitation,[4] many orders of magnitude below other optical techniques. The detection of single or multiple molecules is out of reach except for especially large systems like individual carbon nanotubes.[5,6] The cross section of SERS is by 10^7 to 10^{10} larger than for standard Raman scattering, bringing it on par with the cross section of luminescence.[7-9] SERS detects some molecular species with a sensitivity down to a single molecule.[10] Another advantage of SERS is that its spatial resolution overcomes the diffraction limit. The

diffraction limit restricts the resolution of far-field optical techniques to approximately half the optical wavelength. Because most Raman experiments are performed in the visible and near infrared, their spatial resolution is around some hundred nanometers to a micron. SERS proceeds via optical near-fields bringing the resolution down to the size of the enhancing near-field hotspot, typically tens of nanometers.[11] SERS resolution reaches down to the nanometer level due to the very small hotspots created in the gap between the tip of a scanning tunnelling microscope and a metallic substrate.[12,13]

To harvest the power of SERS for sensing and characterization, one must first obtain an in-depth understanding of its underlying physical principles. Only then, will we be able to optimize its conditions for an envisioned application that may require the highest SERS enhancement, an enhancement that is uniform in space and independent of excitation energy, or require the smallest hotspots for highest spatial resolution. Plasmonic near-fields provide the main enhancement to SERS; they increase the Raman cross section by factors of 10^7 to 10^8.[3,14] Chemical enhancement has its niche in particular combinations of Raman probe and plasmonic material, but its enhancement (up to 10^3) is inferior to the plasmonic contribution.[15,16] Plasmonic enhancement is commonly described within the electromagnetic (EM) enhancement theory. The Raman process in SERS takes place in the EM near fields of metallic nanostructures. These structures sustain pronounced optical resonances that arise from the collective oscillations of their free electrons.[17] The quasi-particle of these excitations is called a localized surface plasmon. Excited plasmons induce strong electric fields close to the nanoparticle, and the energy of the light field is cycled between the oscillating electrons and the confined optical field.[18] The near-field amplitude is by a factor of $E = 10 - 100$ higher than the intensity of the incoming light that excited the plasmon.[19] This increases the Raman intensity due to the higher incoming light amplitude. In addition, the high density of EM states close to the metal particles enhances the amplitude of the scattered outgoing light. Overall, the EM enhancement theory predicts the SERS cross section to increase by a factor $E(\omega_i)^2 E^2(\omega_s)$ compared with the Raman cross section of the material, where ω_i is the frequency of the incoming light and ω_s the frequency of the scattered light in the Raman/SERS process.

Experimental tests of SERS confirmed many predictions of the EM enhancement theory; a review of these achievements is given in other works.[20] For example, nanoparticle agglomerates have a much higher SERS enhancement than individual nanoparticles because the interaction between the near fields of the nanoparticles produces nano-sized hotspots with strong field enhancement.[8,21] The general scaling of the SERS enhancement with nanoparticle size and shape was confirmed experimentally as well.[14] Most of these tests, however, were limited to large molecular ensembles and essentially unknown configurations of plasmonic hot-spots. They provided a relative scaling of the SERS enhancement as opposed to an absolute comparison between theory and experiment. With increasing control over metallic nanostructures, it became feasible to engineer plasmonic hotspots and control their properties. The plasmonic enhancement of a given hotspot can be measured with high precision. In addition to absolute enhancement factors, elaborate predictions like the dependence of the enhancement on excitation wavelength, the spectral width of the enhancement window and its scaling with the inverse plasmon lifetime, and the dependence of the SERS intensity on polarization may be tested experimentally.

In this paper, we discuss rigorous experimental tests of the plasmonic contribution to SERS. The EM theory of plasmonic enhancement explains the underlying principles of SERS. The quantitative predictions of the EM theory, however, fail to describe many SERS effects and the properties of the phenomenon, especially in regard to the total SERS enhancement which is much stronger than predicted. SERS enhancement is found in a narrow wavelength range, in contrast to the broad enhancement window expected by the EM enhancement. Because experimental studies often avoid discussing these shortcomings, an aim of this review is to collect the experimental data that are distributed over many key experimental studies.

2 | PLASMONIC ENHANCEMENT IN SERS

In this section, we briefly introduce the EM enhancement theory and the theory of describing the plasmonic contribution to SERS as a higher order Raman effect.[10,22,23] We also define the various enhancement factors that are used in the experimental and theoretical works. We consider placing a molecule or nanomaterial inside a plasmonic hotspot at position $\mathbf{r}_0$. The metal nanostructure producing the hotspot gets illuminated by far-field radiation with an electric field $\mathbf{E}_{inc}(\mathbf{r}, \omega)$. This induces a Raman dipole with wavenumber ω_s

$$\mathbf{p}_R(\mathbf{r}_0, \omega_s) = \overset{\leftrightarrow}{\alpha}_R(\omega_i, \omega_s) \left[\mathbf{E}_{inc}(\mathbf{r}_0, \omega_i) + \mathbf{E}_{pl}(\mathbf{r}_0, \omega_i) \right] \quad (1)$$

that originates from the incident light field $\mathbf{E}_{inc}$ and the plasmonic near field $\mathbf{E}_{pl}$.[10,19,20] The plasmonic near field

is typically calculated by numerical techniques like finite-difference time-domain or finite-element simulations that include information about the entire plasmonic nanostructure.[20] The plasmonic near field enhances the Raman dipole by a factor $f_{in} = 1 + E = 1 + E_{pl}(\mathbf{r}_0, \omega_i)/E_{inc}(\mathbf{r}_0, \omega_i)$, assuming that the plasmonic near field and the incident field are parallel in polarization. The field that is radiated by the Raman dipole reaches a detector at position $\mathbf{r}_\infty$,

$$\mathbf{E}(\mathbf{r}_\infty, \omega_s) = \frac{\omega_s^2}{\epsilon_0 c^2} \overset{\leftrightarrow}{G}(\mathbf{r}_\infty, \mathbf{r}_0) \mathbf{p}_R(\mathbf{r}_0, \omega_s), \qquad (2)$$

which is calculated with the Green's function of the overall system $\overset{\leftrightarrow}{G}(\mathbf{r}_\infty, \mathbf{r}_0)$ that contains information on the entire plasmonic nanostructure.[19] The Green's function may be split into two parts, a first part that describes the direct radiation of Raman-scattered light into free space $\overset{\leftrightarrow}{G}_0(\mathbf{r}_\infty, \mathbf{r}_0)$ and a second part that describes the emission of the Raman-scattered light via the plasmonic nanostructure $\overset{\leftrightarrow}{G}_{pl}(\mathbf{r}_\infty, \mathbf{r}_0) \approx E_{pl}(\mathbf{r}_0, \omega_s)/E_{inc}(\mathbf{r}_0, \omega_s)\overset{\leftrightarrow}{G}_0(\mathbf{r}_\infty, \mathbf{r}_0)$. By combining Equations (1) and (2), the intensity of the Raman-scattered light is[19]

$$I_{SERS} = \frac{\omega_s^4}{\epsilon_0^2 c^4} \left| \left(1 + \frac{E_{pl}(\mathbf{r}_0, \omega_s)}{E_{inc}(\mathbf{r}_0, \omega_s)} \right) \overset{\leftrightarrow}{G}_0(\mathbf{r}_\infty, \mathbf{r}_0) \overset{\leftrightarrow}{\alpha}_R(\omega_i, \omega_s) \right.$$
$$\left. \mathbf{E}_{inc}(\mathbf{r}_0, \omega_i) \left(1 + \frac{E_{pl}(\mathbf{r}_0, \omega_i)}{E_{inc}(\mathbf{r}_0, \omega_i)} \right) \right|^2. \qquad (3)$$

The amplitudes of the SERS and Raman effect differ by the two factors $f_{in} = 1 + E_{pl}(\mathbf{r}_0, \omega_i)/E_{inc}(\mathbf{r}_0, \omega_i)$ and $f_{out} = 1 + E_{pl}(\mathbf{r}_0, \omega_s)/E_{inc}(\mathbf{r}_0, \omega_s)$. Taken together, they form the EM enhancement factor of the SERS intensity[10,19,20]

$$EF_{em} = \left| \left(1 + \frac{E_{pl}(\mathbf{r}_0, \omega_i)}{E_{inc}(\mathbf{r}_0, \omega_i)} \right) \left(1 + \frac{E_{pl}(\mathbf{r}_0, \omega_s)}{E_{inc}(\mathbf{r}_0, \omega_s)} \right) \right|^2. \qquad (4)$$

When neglecting the Raman shift by setting $\omega_{vib} = 0$ and $\omega_i = \omega_s$ and discarding the direct Raman emission $(E_{pl}/E_{inc} \gg 1)$, the EM enhancement scales with $E^4 = (E_{pl}/E_{inc})^4$, which is known as the E^4 enhancement approximation.

The local field enhancement $E(\mathbf{r}, \omega) = E_{pl}(\mathbf{r}, \omega)/E_{inc}(\mathbf{r}, \omega)$ can be calculated analytically or numerically for almost any plasmonic nanostructure making the EM enhancement theory a powerful tool for the design of SERS substrates with large enhancement.[20] After simulating the local field enhancement of a given nanostructure, the EM enhancement is found by integrating E over the entire surface S

$$EF_{em} = \frac{1}{S} \int_S E^2(\omega_i) E^2(\omega_i - \omega_{vib}) dS. \qquad (5)$$

Instead or in addition to EF_{em}, many simulations report the peak enhancement EF_{max} of a plasmonic system

$$EF_{max} \underset{S}{\max}(E^2(\omega_i) E^2(\omega_s)). \qquad (6)$$

A complementary approach to model the plasmonic enhancement is the description of SERS as a higher order Raman (HORa) process.[22,23] The excitation of the localized surface plasmon is considered as an explicit step in the quantum-mechanical description of the Raman process. The corresponding Feynman diagram includes the interaction between incoming and outgoing photons and plasmons, and the interaction between the plasmon and the vibronic state of the molecules. The Feynman diagram is translated into a Raman scattering amplitude using higher order perturbation theory.[24] The SERS intensity is then obtained from[22,23]

$$I_{SERS} = EF_{HORa}(\omega_i) \cdot I_R, \qquad (7)$$

with the enhancement factor

$$EF_{HORa}(\omega_i) = \left| \frac{\tilde{\mathcal{M}}_{SERS}}{(\omega_i - \omega_{pl} - \omega_{vib} - i\gamma_{pl})(\omega_i - \omega_{pl} - i\gamma_{pl})} \right|^2, \qquad (8)$$

and I_R the Raman intensity. ω_{pl} is the plasmon energy, and γ_{pl} is the inverse plasmon lifetime and corresponds to the spectral width of the plasmonic excitation. $\tilde{\mathcal{M}}_{SERS}$ is a coupling factor that describes the interaction of the incoming and scattered photon, the plasmon and the vibronic states of the molecule. EF_{HORa} can be calculated analytically or numerically using the various interaction Hamiltonians of the HORa process.[22,23]

The analytic expression in Equation (8) is also a powerful tool to analyse the excitation-energy dependence of the SERS signal.[22,23,25,26] The energy denominators describe the plasmonic resonances of the SERS process.[22,23] When the incoming light ω_i matches the plasmon ω_{pl}, the real part of the denominator $(\omega_i - \omega_{pl} - i\gamma_{pl})$ vanishes causing an incoming plasmonic Raman resonance. Similarly, when the scattered light $\omega_i - \omega_{vib}$ matches the plasmon ω_{pl}, the denominator $(\omega_i - \omega_{pl} - \omega_{vib} - i\gamma_{pl})$ vanishes causing an outgoing plasmonic Raman resonance. $\tilde{\mathcal{M}}_{SERS}$, ω_{pl} and γ_{pl} may be used as fitting parameters to extract the properties of the plasmonic excitation from experimental data.[25,26] In contrast to the EM enhancement theory, the HORa

analysis requires no detailed knowledge of the plasmonic nanostructure geometry.

To compare the enhancement theories to experiment, enhancement factors are extracted from experimental data. To do so, the SERS intensity is compared with the Raman intensity of a specific probe. In this paper, we use the surface averaged enhancement, unless explicitly stated otherwise,

$$ \mathrm{EF}_{\mathrm{exp}} = \frac{I_{\mathrm{SERS}} N_{\mathrm{R}}}{I_{\mathrm{R}} N_{\mathrm{SERS}}}, \tag{9} $$

where I_{SERS} is the intensity measured in the SERS experiment on N_{SERS} molecules. I_{R} is the intensity measured in a reference Raman experiment on N_{R} molecules. Measuring SERS and Raman intensity under the same experimental conditions (excitation energy, detection setup etc.) is straightforward. Finding reasonable values for N_{SERS} and N_{R}, however, is a major challenge in quantifying SERS experiments. For the surface averaged enhancement, N_{SERS} is taken to be the total number of molecules on the surface of the plasmonic nanostructure. The surface area is calculated from a high-resolution microscopy image of the nanostructure and multiplied by the surface density of the molecular film. Raman reference measurements are often performed on solutions or powdered samples. N_{R} is then obtained from the focal volume and the concentration or volume density of the molecules. The surface-averaged enhancement $\mathrm{EF}_{\mathrm{exp}}$ is to be compared with $\mathrm{EF}_{\mathrm{em}}$, that is, a surface integration of the local field enhancement. Because $\mathrm{EF}_{\mathrm{exp}}$ refers to all molecules on a plasmonic nanostructure, it underestimates the enhancement in the SERS hotspot, because the hotspot is only a tiny fraction of the total surface. Another approach is, therefore, to estimate the number of molecules in the hotspot N_{hs} and impose that $N_{\mathrm{SERS}} = N_{\mathrm{hs}}$. Finding the number of molecules in the SERS hotspot requires simulations in addition to the experimental input: the extension of the hotspot is obtained from simulation of the local field enhancement. Together with the molecular surface density, this area is converted into N_{hs}. We will refer to such an experimental SERS enhancement as $\mathrm{EF}_{\mathrm{hs}}$. In many studies, $\mathrm{EF}_{\mathrm{hs}}$ is taken as equivalent to $\mathrm{EF}_{\mathrm{max}}$ in the simulations.

3 | PLASMONIC HOTSPOTS

The enhancement of a Raman probe in SERS depends strongly on the exact geometry of the plasmonic hotspot, its strength and the position and orientation of the molecule. These three factors make it very challenging to compare the experimentally observed enhancement in SERS to theoretical predictions. We discuss a number of recent papers that overcame these challenges and provided a quantitative comparison between SERS experiments and theory.

3.1 | Spatial distribution of SERS hotspots

Mapping the spatial distribution of SERS enhancement within a hotspot requires a Raman probe that can be controllably placed at different positions within a hotspot with nanoscale precision. Awada et al.[27] fulfilled this requirement by functionalizing a sharp gold tip with Raman active molecules (4-NTP). The tip was scanned over a semicontinuous gold film with randomly distributed hotspots while recording the molecular SERS enhancement as a function of tip position. As expected, strong enhancement arises from small crevices in the gold film. A precise mapping of the enhancement distribution at a hotspot was impossible because the gold tip acts as an optical antenna. Its interaction with the gold surface creates a dynamic gap-type hotspot whose spatial distribution differs from the surface hotspot. Miranda et al.[28] systematically studied such a gap mode and demonstrated that the gold tip leads to a nontrivial near-field distribution that affects the magnitude of the SERS enhancement and alters the local symmetry selection rules.[29]

In a seminal work, Kusch et al.[11] devised an experimental setup to parallel map the SERS intensity and the EM near field of a SERS hotspot. A grating spectrometer was implemented into a scattering-type scanning near-field optical microscope. An ultrasharp silicon tip mapped the elastically scattering light and served as the Raman probe for SERS. Elastic light scattering gives access to the near-field distribution $E(\omega_{\mathrm{i}})$ in space and allows for a direct comparison with numerical simulations.[11] Raman scattering from the silicon tip (Raman shift $520\,\mathrm{cm}^{-1}$) reveals the local SERS enhancement without altering the local hotspot configuration as was the case for metallic tips.[27] Canonical SERS hotspots formed by plasmonic gold nanodimers were probed using this technique. The dimers consisted of two discs with a conical shape comparable with those shown in Figure 1b further below, which allowed for the silicon tip to reach inside the dimer gap for accurate mapping. Kusch et al.[11] showed that the spatial distribution of the EM field enhancement in the plasmonic hotspots predicts the intensity of the SERS signal and follows the simulations of the local fields. The nanoscale SERS and scanning near-field optical microscope resolution verified that the EM enhancement theory is an excellent tool for calculating SERS hotspots. It may be used to optimize
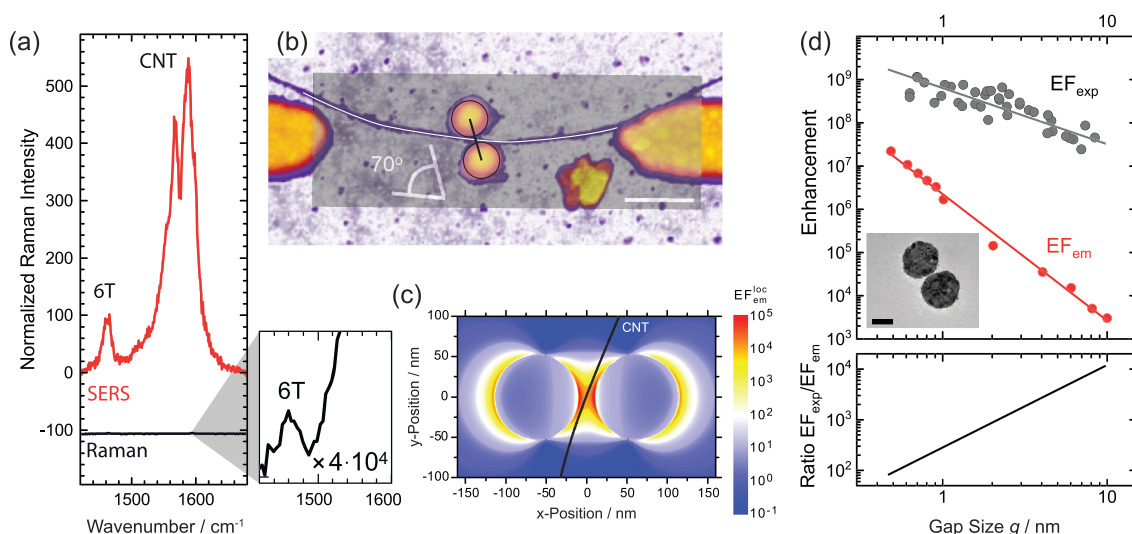
FIGURE 1 (a) SERS (red) and Raman (black) spectra of carbon nanotubes filled with sexithiophene molecules yielding $EF_{exp} = 8 \cdot 10^4$. (b) Atomic force microscopy image of the samples used in the SERS measurements. It is overlaid with the geometrical outline of the nanostructures for the FDTD simulations of local field enhancement in panel (c). (c) Local field enhancement of the gold dimer. An integration along the line of molecules (black line) yields $EF_{em} = 810$. (d) Top: measured (grey) and simulated (red) peak enhancement factors of thiophene on gold dimers (inset) as a function of dimer gap size g. The lines are linear fits. Bottom: ratio between the fits of measured and simulated enhancement over gap size. Panels (a)–(c) are reproduced from Mueller et al.[34] Data in panel (d) are taken from Zhu et al.[33]

nanostructures for a specific distribution, size and shape of SERS hotspot.

3.2 | Absolute measurements of SERS enhancement

Comparing measured enhancement factors to theoretical predictions requires an excellent knowledge of the metal nanostructure that produces the hotspot and the molecular placement. A number of instrumental studies combined SERS and Raman scattering with microscopic images of the plasmonic nanostructures and numerical modelling of the EM enhancement, summarized in Table 1.[30-36] In this table, we included all studies that compared experimental SERS enhancement factors with the EM enhancement theory based on microscopic images of the plasmonic nanostructure. The exact knowledge of the plasmonic system is the crucial point. All such studies used gold nanostructures and red laser excitation. The plasmonic structures were imaged by transmission electron microscopy, scanning electron microscopy or atomic force microscopy. The high-resolution images gave the input geometry for simulations of the surface-averaged EM enhancement EF_{em}, see Equation (5). Except for Mueller et al.,[34] the molecules in these experiments formed films on the nanostructure gold surface. The measured enhancement factors EF_{exp} likewise refer to the entire surface, Equation (9). We note

that the enhanced vibrations fall in a narrow wavenumber range. There are no studies of low-energy phonons $\ll 1000$ cm^{-1} or modes above 2000 cm^{-1}.

The measured SERS enhancement factors range $EF_{exp} = 10^4$-10^8, typically induced by the field in gaps between nanostructures, Table 1. The calculated EF_{em} also span four orders of magnitude 100–10^6. Remarkably, all studies find that the experimental SERS enhancement exceeds the predictions of the EM enhancement theory by two to three orders of magnitude. The EM enhancement theory predicts the relative performance of a plasmonic nanostructure very well but systematically underestimates the total enhancement. In most papers, there is no in-depth evaluation of the discrepancy, which gets attributed to chemical enhancement and surface roughness.[30-33,36] There are two major aspects that make these explanations questionable: first, there is no systematic difference between the EF_{exp}/EF_{em} ratio observed on structures that were produced by wet chemistry and electron-beam lithography. Such a difference is expected if surface roughness was a key parameter. Second, different molecules result in similar ratios between experiment and theory, although chemical enhancement is highly specific to the molecule–surface interaction.[16] Absorption spectra measured on dyes deposited on silver nanoparticles appeared to suggest widespread shifts in the optical spectra of dye molecules on metallic surfaces.[37] However, a follow-up study found this to be an artefact of the halides added as surfactant agents.[38] Gold

TABLE 1 Measured enhancement factors EF_{exp} compared with simulated EF_{em} of the EM enhancement theory

Experimental system	ω_{vib} (cm^{-1})	ω_i (eV)	Exp. EF_{exp}	Theory EF_{em}	Ratio EF_{exp}/EF_{em}	Remark
AuNP trimers (wet chemistry), PCEPE SAM[30]	1582	1.96 (633 nm)	$2 \cdot 10^8$	$1 \cdot 10^6$	200	Simulation for coalesced NPs
AuNPs with interior gap (wet chemistry), Cy3 functionalization[31]	1190	1.96 (633 nm)	$2 \cdot 10^8$	$1 \cdot 10^6$	200	EF_{em} via E^4, peak value reported
Au nanorod dimers (e-beam), BT SAMs, 5 nm gap[32]	1074	1.59 (780 nm)	$7 \cdot 10^7$	$4 \cdot 10^5$	200	
Au nanodisc dimers (e-beam), TP SAM, 2 nm gap[33]	1074	Max. enh.	$3 \cdot 10^8$	$1 \cdot 10^5$	3000	
Same as above, 5 nm gap[33]	1074	Max. enh.	$8 \cdot 10^7$	$2 \cdot 10^4$	4000	
Same as above, 10 nm gap[33]	1074	Max. enh.	$3 \cdot 10^7$	$3 \cdot 10^3$	10 000	
Au nanodisc dimer (e-beam), $\alpha-6T$ aligned in nanotubes, 20 nm gap[34]	1450	1.94 (638 nm)	$8 \cdot 10^4$	$8 \cdot 10^2$	100	
Au NP@mirror, TPT SAM[35]	1585	Not given	10^8	$10^6 - 10^7$	≈ 100	Only order of magnitude given
Au ellipsoid (single, wet chemistry), spin-coated BT[36]	1072	1.92 (647 nm)	$8 \cdot 10^6$	$7 \cdot 10^4$	110	

Note: The first column sketches the experimental system. The enhancement factors EF_{exp} were reported for a given Raman shift ω_{vib} and excitation energy ω_i. Zhu et al.[33] measured enhancement profiles and reported the highest enhancement observed.

Abbreviations: 6T, sexithiophene; BT, benzenethiol; e-beam, electron-beam lithography; NP, nanoparticle; PCEPE, 2-(4-pyridyl)-2-cyano-1-(4-ethynylphenyl) ethylene; SAM, self-assembled monolayer; TP, thiophenol; TPT, terphenyl-thiol.

nanoparticles induced no changes to the optical response of the dyes (other than in intensity). If anything, resonant molecules like Cy3 were expected to lower their Raman cross section by chemical interaction. However, the SERS enhancement of Cy3 is again higher than calculated,[31] see Table 1.

Two of the experiments provide further insight into the relation between experimental SERS enhancement and the EM enhancement theory. Mueller et al.[34] measured SERS enhancement on α-sexithiophene (α-6T) molecules that were filled into single-walled carbon nanotubes,[6] Figure 1a. This is a remarkable Raman probe for SERS, because it allows the determination of the exact position and orientation of the molecules in the microscopy images via the carbon nanotube, Figure 1b. The 20 nm gaps in the Au dimer ensured >1 nm separation between the molecules and the gold. Chemical enhancement and surface roughness could, therefore, be excluded as major enhancement mechanisms in the experiments. Nevertheless, Mueller et al.[34] found the EF_{exp} to exceed the EM predictions by a factor of 100, Figure 1a,c, very similar to the other studies in Table 1. Zhou and Crozier[33] observed a dependence of EF_{exp}/EF_{em} on dimer gap size, Figure 1d. This cannot be explained by chemical enhancement or surface roughness: the discs forming the dimers were identical in their roughness regardless of the gap. Also, roughness would yield

additional SERS enhancement for very small gaps, because surface protrusions of the two discs get close and form mini-hotspots. Nothing like this is evident from the experimental data.[33] The thiophene molecules were anchored to the gold surface via thiol groups; chemical enhancement is, therefore, also independent of gap size. We propose that the stronger experimental SERS enhancement is a consequence of collective effects arising from the plasmonic coupling, which have not been identified so far. Although we cannot provide a physical explanation for the phenomenon, we noted an interesting scaling of the experimental data with the number of molecules in the SERS hotspot. In the following, we show how this scaling removes the quantitative discrepancies between experimental SERS enhancement and the EM theory for a number of studies with distinct SERS configurations and Raman probes.

A fundamental assumption that underlies the analysis of the experimental SERS data is that the intensity from the various molecules adds up incoherently, see Equation (9), that is, the intensity of N molecules equals N times the intensity of a single molecule. The intensity of spatially coherent scattering, in contrast, scales with N^2.[39] Plasmonic antennas indeed induced spatially coherent scattering in two-dimensional materials.[40,41] Beams et al.[40] showed experimentally how the approach curves in plasmonic tip-enhanced Raman scattering

changed due to coherent scattering. They also observed novel selection rules in tip-enhanced Raman scattering that were characteristic of a coherent Raman response.[29,39,40] Another interesting case was that spatially coherent scattering was suggested to occur in a molecular film in an optical cavity.[42] Shalabney et al.[42] matched the energies of a silver cavity and the vibration of a polyvinyl acetate film. The strong light-matter coupling between the infrared vibrational transitions and the cavity modes increased the Raman intensity by several orders of magnitude. The authors proposed spatial coherence of the hybrid infrared light-matter state as a possible origin of the enhanced Raman response,[42] although this explanation was challenged in theoretical studies (no alternative explanation for the experimental results has been put forward).[43] Another effect that gives rise to N^2 scaling is cooperative Raman scattering, that is, the equivalent process to superradiance in inelastic light scattering. Hu and Huang[44] found the cooperative Raman effect to scale with the number of molecules in the vibrationally excited state. Similar effects were recently studied within the framework of molecular optomechanics.[45,46] For high-wavenumber vibrations, cooperativity needs a population of the vibrational states that is strongly out of thermal equilibrium.[45,47] The plasmonic enhancement required to populate the vibrational states beyond unity cannot be reached with the EFs listed in Table 1.[45,47-49]

In a pragmatic approach, we now examine how N^2 scaling will affect the measured EF in Table 1 and their comparison with simulation. We describe the SERS intensity as the sum of an enhanced intensity originating from the plasmonic hotspot and the background Raman intensity from the remaining metal nanostructure. Although the Raman part scales linearly with the number of molecules N_d, the hotspot intensity scales as the number of molecules in the hotspot squared N_{hs}^2

$$I_{SERS} = N_{hs}^2 \sigma_{SERS} + N_d \sigma_R, \quad (10)$$

where σ_R is the Raman cross section, $\sigma_{SERS} = EF_{N^2} \cdot \sigma_R$ is the enhanced SERS cross section, and EF_{N^2} the desired enhancement factor. Comparing Equation (10) to the standard definition of enhancement EF_{exp} in Equation (9) and assuming a negligible contribution of the Raman scattering background, we find

$$EF_{N^2} = \frac{1}{N_d} \left(\frac{N_d}{N_{hs}} \right)^2 EF_{exp}. \quad (11)$$

Equation (11) will allow converting experimental enhancement factors into the enhancement with N^2

scaling. The conversion for the simulated enhancement is obtained by correcting the averaged simulated enhancement by the ratio of the total surface area S and the area of the hotspot S_{hs}, that is, $EF_{hs,em} = S/S_{hs} \cdot EF_{em}$.

Mueller et al.[34] provided all necessary data to calculate the enhancement assuming N^2 scaling directly from their paper ($N_d = 5500$, $N_d/N_{hs} = 38$). We find $EF_{N^2} = 2 \cdot 10^4$ for the measured and $EF_{hs,em} = 3 \cdot 10^4$ for the simulated enhancement, which is an excellent agreement keeping in mind the uncertainties in the experimental part. The plasmonic enhancement studied by Zhu and Crozier,[33] Figure 1d, has an implicit dependence on the size of the hotspot (and thus the number of molecules), because the hotspot area increases with dimer gap. Based on the experimental data provided by Zhu et al.,[33] we simulated the local field enhancement, Figure 2a, and the hotspot area as the dimer surface fraction that accounts for 68% of the averaged enhancement; the area increases like $g^{0.78}$ with gap size g, see Figure 2b. The total number of molecules on the dimer is approximately $1.6 \cdot 10^5$, see supporting information of Zhu et al.[33] We calculate the measured EF_{N^2} and simulated enhancement $EF_{hs,em}$ from the data in Figure 1d. Evaluated in this way, the experimental and simulated data agree very well, Figure 2c. The small drop of the experimental data for the smallest gap sizes comes from the onset of quantum effects; for example, electrons tunnelling through the Å-sized dimer gap.[33] Scaling the SERS intensity with N^2 describes the experimental enhancement surprisingly well.

Summarizing, measured SERS enhancement factors exceed the predictions of the EM enhancement theory by two to three orders of magnitude, see Table 1 and Figure 1. The common explanation of an additional contribution arising from chemical enhancement and surface roughness appears questionable in view of the consistent discrepancy from various molecules and plasmonic nanostructures. The experimental basis would be strengthened by a greater variety of plasmonic materials and by studying Raman peaks below 1000 cm^{-1}. We examined a potential scaling of the SERS intensity with the square of the Raman probes as is characteristic for spatially coherent scattering. When including this additional contribution to the SERS intensity, we found excellent agreement between the measured and predicted enhancement.

4 | PLASMONIC RESONANCES IN SERS

In this section, we collect and discuss experiments on the excitation energy-dependence of the SERS enhancement.
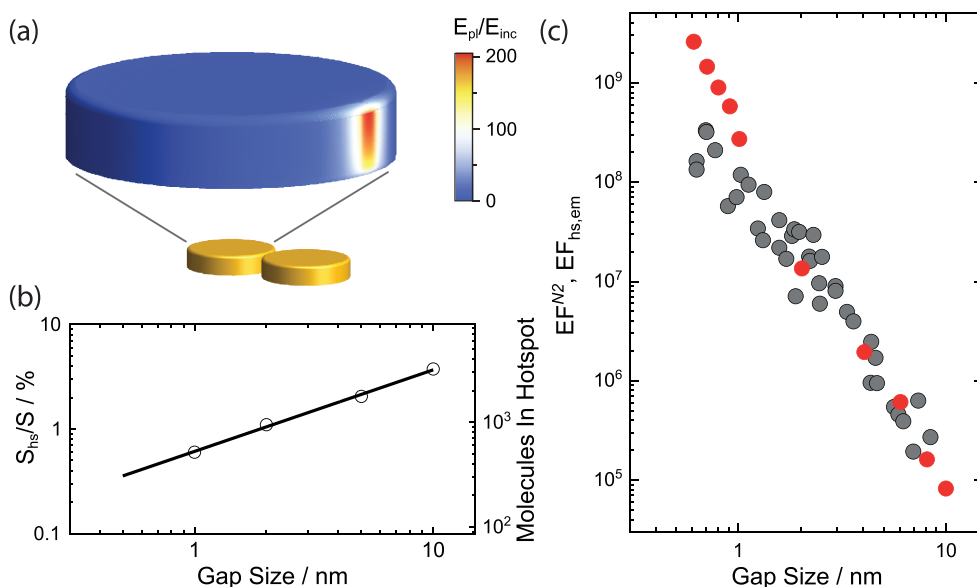
FIGURE 2 (a) Simulated local field enhancement in a dimer with 1 nm gap, see Appendix B1. We define the hotspot as the area that accounts for 68% of the total E^4 enhancement. (b) Surface fraction (left) and number of molecules (right) in the hotspot as a function of gap size g. For the number of molecules, we used a surface density $\rho_s = 6.8 \cdot 10^{14}$ cm^{-1}.[33] (c) EF$_{N^2}$ (grey) and EF$_{hs, em}$ (red) as a function of gap size, that is, assuming N^2 scaling of the scattering intensity in the hotspot. Compare with Figure 1d where the data were evaluated for linear scaling of the intensity in the hotspot

By how much a plasmonic nanostructure enhances the incoming or scattered electric field depends on the energy of the EM radiation.[17] An enhancement occurs if the energy matches the plasmon resonance within the plasmonic line width.[22,23] SERS is caused by the excitation of optically bright, dipole-allowed plasmons with very strong far-field coupling. Such modes have a line width (full width at half maximum, FWHM) of several 100 meV. The decay is typically dominated by radiative damping. There are ways to excite dipole-inactive modes in plasmonic structures through field retardation and tailored light-fields,[50,51] but here, we focus on linearly polarized light and plasmonic structures that may be described within the quasi-static approximation. The plasmon resonance with a width of several 100 meV leads to a predicted EM enhancement with a FWHM of ≈300 meV for many gold nanostructures, see Figure 3a. The simulations were done for ideal structures without imperfections, roughness, substrates and ligands.[30,34] These additional features are present in real plasmonic nanostructures and inevitably further increase the enhancement line width. For example, we repeated the simulations of the Au dimer with a 30 nm gap (light grey in Figure 3a) when placing the dimer on a Cr interlayer and a SiO$_2$/Si substrate as is typical for plasmonic structures from electron-beam lithography. The simulated linewidth of the EM enhancement profile increased from 300 meV for the free standing structure in Figure 3a (30
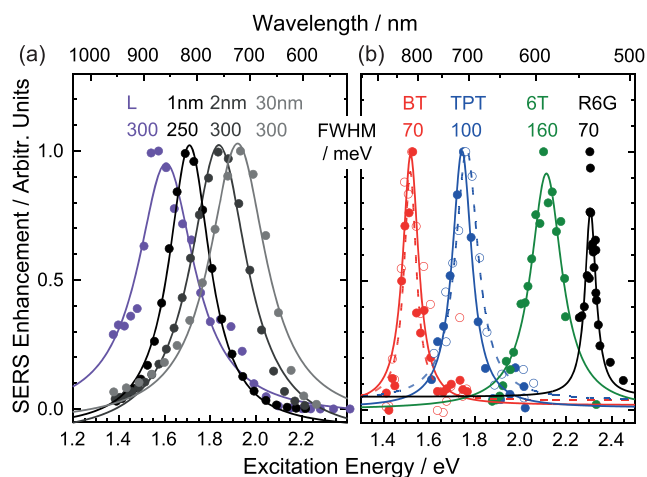

FIGURE 3 Plasmonic resonances in (a) simulations and (b) experiment. (a) Simulated EM enhancement as a function of excitation energy for various nanostructures: L, L-shaped trimer; 1 nm, dimer with 1 nm gap size; 2 nm, dimer with 2 nm gap size (all from Wustholz et al.[30]); 30 nm, dimer with 30 nm gap (see Appendix B1). The numbers indicate the FWHM for a fit by a single Lorentzian. (b) Measured SERS enhancement as a function of excitation energy for BT on Au nanodimers[33] (open and closed symbols refer to Dimer II and Dimer III of the reference), TPT in a nanoparticle on a mirror configuration[35] (open and closed symbols refer to the mode at 1080 and 1585 cm^{-1}), 6T encapsulated in a nanotube and placed in a Au nanodimer,[26] and R6G on a colloidal Ag surface.[21] The numbers indicate the FWHM if the data is fit by a single Lorentzian

nm, light grey) to 500 meV on top of the adhesion layer and the substrate (not shown). Due to the large plasmon line width, SERS was predicted to enhance light scattering in a broad range of excitation energies.

We now compare the simulations with experiments where the SERS intensity from an individual hotspot was recorded as a function of laser excitation energy.[21,25,26,33,35] The measured SERS enhancement profiles are much narrower, Figure 3b, than expected from the EM enhancement theory, Figure 3a. The FWHM of the resonance profiles was always well below 200 meV and as small as 70 meV.[21,25,26,33,35] The surprisingly narrow linewidth of the SERS enhancement is a second remarkable discrepancy between the predictions of the EM enhancement theory and the experimental findings. The quality factor $Q = \omega_{pl}/FWHM$ of the resonances in Figure 3b is close to 20, exceeding the theoretical maximum allowed for gold within the quasi-static approximation.[53] Although this upper limit is no longer strictly valid if field retardation is considered, retardation leads to radiation as an additional damping mechanism further increasing the FWHM.[51] Most studies of SERS enhancement profiles did not comment on the narrow resonances. Dieringer et al.[21] argued that the small width of the R6G resonance on a colloidal silver surface (black dots in Figure 3b was due to a molecular resonance. Zhu and Crozier[33] (red) and Wasserroth et al.[26] (green), however, ruled out molecular resonances at the energy of the SERS resonance through reference measurements without plasmonic enhancement. Lombardi et al.[35] (blue) showed that their resonance is plasmonic and not molecular: changing the plasmonic nanostructure shifted the SERS maximum up by 150 meV following the plasmon energy.

An interesting study examined how the molecular resonance interplays with the plasmon resonance in a SERS enhancement profile, Figure 4. SERS was measured on a carbon nanotube that lay in the nanocavity of a plasmonic gold dimer, see Appendix B1.[52] The experiment controlled the polarization of the incoming and scattered light. When the polarization was along the nanotube axis, there was no plasmonic enhancement. The corresponding Raman spectrum (black) is shown in Figure 4. The radial breathing mode (RBM) had a strong Raman intensity around ~1.93 eV, because of the intrinsic excitonic resonance of the (7,5) nanotube.[5,54,55] A fit of the Raman resonance profile yields an exciton resonance at 1.92 eV with a FWHM $\gamma_{exc} = 80$ meV in excellent agreement with earlier measurements.[52,55] The resonance profile in Figure 4b appears broader than 100 meV, because the incoming and outgoing Raman resonances overlap. Now the polarization was turned to be along the axis of the nanodimer. The incoming and scattered light couple to the superradiant bright plasmon of the dimer. The corresponding SERS spectrum (red) in Figure 4a shows the same peaks as the spectrum in the absence of plasmonic enhancement (black) but with different intensities. This is the typical behaviour of one-dimensional systems like carbon nanotubes where only fully symmetric phonons are Raman active.[34,56-58] The SERS profile, Figure 4c, is a superposition of the intrinsic nanotube resonance plus the plasmonic SERS resonance. A fit of the SERS profile with Equation (7) yields a plasmon resonance at 1.91 eV with $\gamma_{pl} = 80$ meV. Interestingly, the SERS profile in Figure 4c appears narrower than the intrinsic Raman resonance in panel (b), because the intrinsic and plasmonic resonance act simultaneously. This was confirmed in a study of SERS
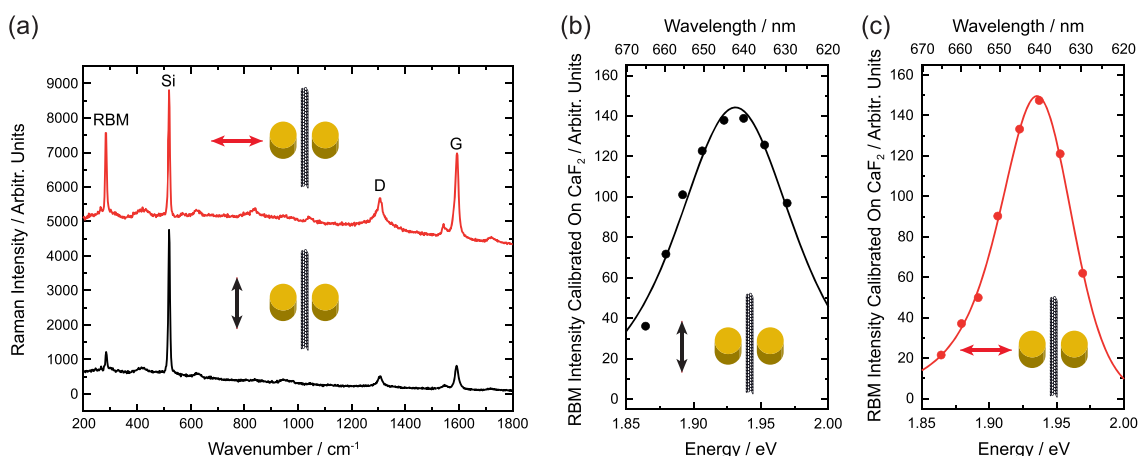

FIGURE 4 Resonances in SERS and Raman scattering on a carbon nanotube. (a) Raman (black) and SERS spectrum (red) of a carbon nanotube placed in a plasmonic gold dimer for $\lambda = 638$ nm. The Raman or SERS character of light scattering is selected by turning the polarization direction of the exciting laser. (b) Raman and (c) SERS intensity of the radial breathing mode (RBM) in a carbon nanotube as a function of excitation energy. From Ref.[52]

and Raman resonances in 6T molecules: The molecular resonance had a FWHM (130 meV) that exceeded the width of the plasmonic resonance (70 meV) by almost a factor of two.[26] The narrow resonance width is an intrinsic property of the SERS effect.

SERS enhancement profiles have a narrow line width of typically 100 meV and less, Figures 3b and 4c, which contradicts the broad plasmonic resonances measured in dark-field spectroscopy and extracted from simulations, Figure 3a. The narrow resonances are not caused by intrinsic molecular resonances, because they appear irrespective of the molecular properties. A nonthermal vibrational population through extremely strong SERS enhancement was suggested to narrow the enhancement profiles.[45,46] However, reaching this regime requires tiny mode volumes or very strong light-matter coupling,[47,48] which was not realized in the studies underlying Figures 3 and 4. Another idea to explain narrow SERS resonances is the contribution of dark modes in the scattering process. Dark modes are plasmonic excitations with vanishing dipole moment.[59,60] They are optically inactive within the quasi-static approximation but can be excited due to field retardation, by misalignment of Gaussian beams and by structured light.[50,51,60,61] Dark modes have smaller line width by approximately a factor of two,[51] which would bring the expected width of the SERS resonances much closer to the experimental values, Figure 3. This suggestion, however, has to explain why the SERS process is dominated by dark modes at the expense of the bright plasmons.

5 | CONCLUSION

Surface-enhanced Raman scattering is an intriguing analytic technique with many applications in the life and physical sciences and, potentially, industrial settings. It is clear that the largest contribution to the SERS enhancement is from localized surface plasmons and their EM near fields. The so-called EM enhancement theory describes SERS as a Raman effect that gets enhanced by the increase in the local electric field and the change in the density of EM states. The theory of EM enhancement explains why metallic nanostructures strongly increase the cross section for inelastic light scattering. In this paper, we reviewed a set of experiments that test advanced predictions of the EM enhancement theory. We find that it correctly predicts the shape and size of SERS hotspots. The EM enhancement theory, however, consistently underestimates the magnitude of the SERS effect by several orders of magnitude. It also predicts an energy window for SERS enhancement that is by a factor of three to five broader than observed experimentally. These experimental results challenge further theoretical work. Collective effects that arise from the plasmonic and molecular coupling appear to be a promising route to pursue. Recent proposals examined the regime for cooperative emission in SERS through a nonlinear increase in phonon population. Although the predicted phenomena would explain the additional enhancement found in experiment and its narrow line width, the stringent conditions for reaching the regime are beyond the standard SERS experiments discussed here. The goal of this paper was to scrutinize recent experiments that examined SERS in a quantitative way under carefully controlled experimental conditions. We would like to open a discussion within the scientific community on how to further develop the theoretical description of surface-enhanced Raman scattering.

ORCID

Sebastian Heeg https://orcid.org/0000-0002-6485-3083
Niclas S. Mueller https://orcid.org/0000-0002-8688-1974
Sören Wasserroth https://orcid.org/0000-0002-3645-5969
Patryk Kusch https://orcid.org/0000-0001-9180-786X
Stephanie Reich https://orcid.org/0000-0002-2391-0256

REFERENCES

[1] P. L. Stiles, J. A. Dieringer, N. C. Shah, R. P. Van Duyne, *Annu. Rev. Anal. Chem.* **2008**, *1*(1), 601.

[2] B. Sharma, R. R. Frontiera, A.-I. Henry, E. Ringe, R. P. Van Duyne, *Mater. Today* **2012**, *15*(1), 16.

[3] J. Langer, D. Jimenez de Aberasturi, J. Aizpurua, R. A. Alvarez-Puebla, B. Auguié, J. J. Baumberg, G. C. Bazan, S. E. J. Bell, A. Boisen, A. G. Brolo, J. Choo, D. Cialla-May, V. Deckert, L. Fabris, K. Faulds, F. J. García de Abajo, R. Goodacre, D. Graham, A. J. Haes, C. L. Haynes, C. Huck, T. Itoh, M. Käll, J. Kneipp, N. A. Kotov, H. Kuang, E. C. Le Ru, H. K. Lee, J.-F. Li, X. Y. Ling, S. A. Maier, T. Mayerhöfer, M. Moskovits, K. Murakoshi, J.-M. Nam, S. Nie, Y. Ozaki, I. Pastoriza-Santos, J. Perez-Juste, J. Popp, A. Pucci, S. Reich, B. Ren, G. C. Schatz, T. Shegai, S. Schlücker, L.-L. Tay, K. G. Thomas, Z.-Q. Tian, R. P. Van Duyne, T. Vo-Dinh, Y. Wang, K. A. Willets, C. Xu, H. Xu, Y. Xu, Y. S. Yamamoto, B. Zhao, L. M. Liz-Marzán, *ACS Nano* **2019**, *14*, 28.

[4] M. Cardona, *in Light scattering in solids II*, Springer, New York **1982**, 19, 173.

[5] C. Thomsen, S. Reich, *in Light scattering in solid IX*, (Eds: M. Cardona, R. Merlin), Springer, New York **2007**, 115–235.

[6] E. Gaufrès, N. Y. W. Tang, F. Lapointe, J. Cabana, M. A. Nadon, N. Cottenye, F. Raymond, T. Szkopek, R. Martel, *Nat. Photonics* **2013**, *8*(1), 72.

[7] E. C. Le Ru, B. E, M. Meyer, P. G. Etchegoin, *J. Phys. Chem. C* **2007**, *111*(37), 13794.

[8] Y. Fang, N.-H. Seong, D. D. Dlott, *Science* **2008**, *321*, 388.

[9] T. A. Laurence, G. B. Braun, N. O. Reich, M. Moskovits, *Nano Lett.* **2012**, *12*(6), 2912.

[10] E. C. L. Ru, P. G. Etchegoin, *Principles of surface-enhanced raman spectroscopy*, Elsevier, Amsterdam **2009**.

[11] P. Kusch, S. Matel, N. M. Azpiazu, S. Heeg, R. Gobrachev, F. Schedin, U. Hübner, J. I. Pascual, S. Reich, R. Hillenbrand, *Nano Lett.* **2017**, *17*, 2667.

[12] R. Zhang, Y. Zhang, Z. C. Dong, S. Jiang, C. Zhang, L. G. Chen, L. Zhang, Y. Liao, J. Aizpurua, Y. Luo, J. L. Yang, J. G. Hou, *Nature* **2013**, *498*(7452), 82.

[13] J. Lee, K. T. Crampton, N. Tallarida, V. A. Apkarian, *Nature* **2019**, *568*, 78.

[14] M. Moskovits, *Phys. Chem. Chem. Phys.* **2013**, *15*, 5301.

[15] S. M. Morton, L. Jensen, *J. Am. Chem. Soc.* **2009**, *131*, 4090.

[16] L. Jensen, C. M. Aikens, G. C. Schatz, *Chem. Soc. Rev.* **2008**, *37*, 1061.

[17] S. A. Maier, *Plasmonics: Fundamentals and applications*, Springer, New York **2007**.

[18] J. B. Khurgin, *Nat. Nanotech.* **2015**, *10*, 2.

[19] L. Novotny, B. Hecht, *Principles of nano-optics*, 2nd ed., Cambridge University Press, Cambridge **2012**.

[20] S.-Y. Ding, E.-M. You, Z.-Q. Tian, M. Moskovits, *Chem. Soc. Rev.* **2017**, *46*, 4042.

[21] J. A. Dieringer, K. L. Wustholz, D. J. Masiello, J. P. Camden, S. L. Kleinman, G. C. Schatz, R. P. V. Duyne, *J. Am. Chem. Soc.* **2009**, *131*, 849.

[22] N. S. Mueller, S. Heeg, S. Reich, *Phys. Rev. A* **2016**, *94*, 23813.

[23] N. S. Mueller, S. Reich, *Front. Chem.* **2019**, *7*, 470.

[24] P. Y. Yu, M. Cardona, 4th ed., Springer, Berlin **2010**.

[25] S. Wasserroth, T. Bisswanger, N. S. Mueller, P. Kusch, S. Heeg, N. Clark, F. Schedin, R. Gorbachev, S. Reich, *Phys. Rev. B* **2018**, *97*, 155417.

[26] S. Wasserroth, S. Heeg, N. S. Mueller, P. Kusch, U. Hübner, E. Gaufrès, N. Y.-W. Tang, R. Martel, A. Vijayaraghavan, S. Reich, *J. Phys. Chem. C* **2019**, *123*(16), 10578.

[27] C. Awada, J. Plathier, C. Dab, F. Charra, L. Douillard, A. Ruediger, *Phys. Chem. Chem. Phys.* **2016**, *18*, 9405.

[28] H. Miranda, C. Rabelo, L. G. Cançado, T. L. Vasconcelos, B. S. Oliveira, F. Schulz, H. Lange, S. Reich, P. Kusch, A. Jorio, *Phys. Rev. Research* **2020**, *2*, 23408. https://link.aps.org/doi/10.1103/PhysRevResearch.2.023408

[29] A. Jorio, N. S. Mueller, S. Reich, *Phys. Rev. B* **2017**, *95*, 155409.

[30] K. L. Wustholz, A.-S. Henry, J. M. McMahon, R. G. Freeman, N. Valley, M. E. Piotti, M. J. Natan, G. S. Schatz, R. P. van Duyne, *J. Am. Chem. Soc.* **2010**, *132*, 10903.

[31] D.-K. Lim, K.-S. Jeon, J.-H. Hwang, H. Kim, S. Kwon, Y. D. Suh, J.-M. Nam, *Nat. Nanotechnol.* **2011**, *6*, 452.

[32] W. Zhu, M. G. Banaee, D. Wang, Y. Chu, K. B. Crozier, *Small* **2011**, *7*, 1761.

[33] W. Zhu, K. B. Crozier, *Nature Commun.* **2014**, *5*, 5228/1.

[34] N. S. Mueller, S. Heeg, P. Kusch, E. Gaufrès, N. Y.-W. Tang, U. Hübner, R. Martel, A. Vijayaraghavan, S. Reich, *Faraday Discuss.* **2017**, *205*, 85.

[35] A. Lombardi, A. Demetriadou, L. Weller, P. Andrae, F. Benz, R. Chikkaraddy, J. Aizpurua, J. J. Baumberg, *ACS Photonics* **2016**, *3*, 471.

[36] D. Talaga, M. Comesana-Hermo, S. Ravaine, R. A. L. Vallee, S. Bonhommeau, *J. Opt.* **2015**, *17*, 114006/1.

[37] B. L. Darby, B. Auguié, M. Meyer, A. E. Pantoja, E. C. Le Ru, *Nat. Photonics* **2016**, *10*, 50.

[38] V. Petráková, I. C. Sampaio, S. Reich, *J. Phys. Chem. C* **2019**, *123*(28), 17498.

[39] L. G. Cançado, R. Beams, A. Jorio, L. Novotny, *Phys. Rev. X* **2014**, *4*, 31054.

[40] R. Beams, L. G. Cançado, S.-H. Oh, A. Jorio, L. Novotny, *Phys. Rev. Lett.* **2014**, *113*, 186101.

[41] R. S. Alencar, C. Rabelo, H. L. S. Miranda, T. L. Vasconcelos, B. S. Oliveira, A. Ribeiro, B. C. Públio, J. Ribeiro-Soares, A. G. S. Filho, L. G. Cançado, A. Jorio, *Nano Lett.* **2019**, *19*(10), 7357.

[42] A. Shalabney, J. George, H. Hiura, J. A. Hutchison, C. Genet, P. Hellwig, T. W. Ebbesen, *Ang. Chem.* **2015**, *54*, 7971.

[43] J. del Pino, J. Feist, F. J. Garcia-Vidal, *J. Phys. Chem. C* **2015**, *119*, 29132.

[44] C.-K. Hu, C.-Y. Huang, *Opt. Commun.* **1982**, *43*, 935.

[45] P. Roelli, C. Galland, N. Piro, T. J. Kippenberg, *Nat. Nanotechnol.* **2015**, *11*, 164.

[46] M. K. Schmidt, R. Esteban, A. González-Tudela, G. Giedke, J. Aizpurua, *ACS Nano* **2016**, *10*, 6291.

[47] F. Benz, M. K. Schmidt, A. Dreismann, R. Chikkaraddy, Y. Zhang, A. Demetriadou, C. Carnegie, H. Ohadi, B. deNijs, R. Estaban, J. Aizpura, J. J. Baumberg, *Science* **2016**, *354*, 726.

[48] A. Lombardi, M. K. Schmidt, L. Weller, W. M. Deacon, F. Benz, B. de Nijs, J. Aizpurua, J. J. Baumberg, *Phys. Rev. X* **2018**, *8*, 11016.

[49] Y. Zhang, J. Aizpurua, R. Esteban, *ACS Photonics* **2020**, *7*(7), 1676.

[50] N. S. Mueller, B. G. M. Vieira, F. Schulz, P. Kusch, V. Oddone, E. B. Barros, H. Lange, S. Reich, *ACS Photonics* **2018**, *5*(10), 3962.

[51] S. Reich, N. S. Mueller, M. Bubula, *ACS Photonics* **2020**, *7*, (6), 1537.

[52] S. Wasserroth. **2019**, Plasmon-enhanced raman scattering of carbon nanosystems, Ph.D. Thesis, Freie Universität Berlin.

[53] F. Wang, Y. R. Shen, *Phys. Rev. Lett.* **2006**, *97*, 206806.

[54] H. Telg, J. Maultzsch, S. Reich, F. Hennrich, C. Thomsen, *Phys. Rev. Lett.* **2004**, *93*, 177401.

[55] J. Maultzsch, H. Telg, S. Reich, C. Thomsen, *Phys. Rev. B* **2005**, *72*, 205438.

[56] S. Heeg, A. Oikonomou, R. Fernández-García, C. Lehmann, S. A. Maier, A. Vijayaraghavan, S. Reich, *Nano Lett.* **2014**, *14*, 1762.

[57] S. Heeg, N. Clark, A. Oikonomou, A. Vijayaraghavan, S. Reich, *Phys. Stat Solidi (RRL)* **2014**, *8*(9), 785.

[58] S. Heeg, N. Clark, A. Vijayaraghavan, *Nanotechnology* **2018**, *29*(46), 465710.

[59] J. Sancho-Parramon, S. Bosch, *ACS Nano* **2012**, *6*, 8414.

[60] D. E. Gomez, Z. Q. Teo, M. Altissimo, T. J. Davis, S. Earl, A. Roberts, *Nano Lett.* **2013**, *13*, 3722.

[61] G. Volpe, S. Cherukulappurath, R. J. Parramon, G. Molina-Terriza, R. Quidant, *Nano Lett.* **2009**, *9*, 3608.

[62] E. D. Palik, *Handbook of optical constants of solids*, Academic Press Handbook Series, Academic Press, Burlington **1985**.

[63] P. B. Johnson, R. W. Christy, *Phys. Rev. B* **1972**, *6*, 4370.

[64] S. Heeg, R. Fernández-García, A. Oikonomou, F. Schedin, R. Narula, S. A. Maier, A. Vijayaraghavan, S. Reich, *Nano Lett.* **2013**, *13*, 301.

APPENDIX A: DATA AND METHODS

This paper contained data that we took from previous studies in the literature, unpublished data from our own group and experiments that were presented as part of a PhD thesis. In this section, we will specify the origin of the digitized data and present the methods for the unpublished experiments and simulations. All data can be found in the repository REFUBIUM, under identifier https://doi.org/10.17169/refubium-27805.

Digitized data: We digitized published data using the software WebPlotDigitizer. Figure 1c contains data from Zhu and Crozier.[33] The grey dots are from Figure 4a and the red dots from Figure 4b of the reference. The enhancement factors were extracted for gap sizes 1–10 nm. The lines are fits to the digitized data. Figure 3a contains the simulated SERS resonance curves of an L-shaped trimer, a dimer with 1 nm and a dimer with 2 nm gap size that were taken from Wustholz et al.[30] The purple dots are from Figure 3b (dots, right axis), the black dots from Figure 5d (red line) and the dark grey dots from Figure 5d (black line) of the reference. The light grey data in Figure 3a were calculated by us for a gold dimer with $g = 30$ nm gap size. Details on the simulations are given further below. All simulated data sets were normalized to one at maximum enhancement. Figure 3b contains experimental data from various sources; the data were digitized and then normalized to the maximum enhancement value: The closed (open) red dots are from Figure 3b (Figure 3a) of Zhu and Crozier.[33] The blue dots were taken from NP2 in Figure 3a of Lombardi et al.;[35] closed (open) dots represent the enhancement measured for the 1585 cm^{-1} (1080 cm^{-1}) mode. The green dots are from Figure 6b of Wasserroth

et al.[26] The black dots were extracted from Figure 4c by Dieringer et al.[21]

Simulations: Simulations were performed using the commercial software package Lumerical FDTD Solutions. The field amplitude enhancement in Figure 2a was simulated by reconstructing the geometry of the gold nanodisc dimer in Zhu et al.[33] Two Au discs of 90 nm diameter and 20 nm height were placed 1 nm apart. The upper edge of the Au discs was rounded with a curvature radius of 3 nm. The Au discs were positioned on top of two 1 nm thick Ti discs with 94 nm diameter. The dimer was placed on a 30 nm thick layer with refractive index $n = 2$ to mimic the SiN substrate in the experiments. A 0.25 nm mesh was used to discretize space close to the dimer. The materials were modelled by fitting the dielectric functions of Au and Ti from Palik.[62] The dimer was illuminated with linearly polarized light from the top and polarization along the dimer axis using a total-field scattered-field source. The electric field enhancement was evaluated at a distance of 0.5 nm to the gold surface with a curved point-monitor analysis group at the wavelength $\lambda = 867$ nm of maximum field enhancement. The total SERS enhancement was calculated as the surface average of the E^4 enhancement based on the data shown in Figure 2a. The fractional surface area of the plasmonic hotspot, see Figure 2b, was then calculated as the area that accounts for 68% of the total SERS enhancement. The data points for dimers with 2, 5, and 10 nm gaps were obtained in a similar way.

The wavelength-dependent field enhancement of an Au nanodimer with 30 nm gap in Figure 3a was simulated as follows. The Au discs had a diameter of 100 nm and a height of 40 nm. A 0.5 nm mesh was used to discretize space close to the dimer. The dielectric function of Au was modelled by a fit of experimental data from Johnson and Christy.[63] The refractive index of the medium surrounding the dimer was set to $n = 1$. The dimer was illuminated with linearly polarized light from the top and polarization along the dimer axis using a total-field scattered-field source. The field enhancement was recorded by a point monitor positioned in the hotspot of the dimer. The SERS enhancement in Figure 3a was calculated with Equation (4) assuming a Raman shift of $\omega_{\text{vib}} = 0.2$ eV. We also simulated the SERS enhancement for a dimer with realistic substrate, that is, 4 nm thick Cr discs below the gold and a substrate that consisted of 300 nm SiO$_2$ and Si below. We extracted a spectral width of 480 meV from a fit of the simulated enhancement profile.

Experiment: The experimental data on the polarization dependence of the SERS and Raman resonance in carbon nanotubes were taken from the PhD Thesis of S. Wasserroth.[52] Briefly, the nanotubes of (7,5) chirality were deposited in a gold nanodisc dimer using

dielectrophoresis.[6,26,52,56] SERS and Raman scattering were excited with fully tunable dye lasers that were focused on the nanodimer by a 100× objective (NA 0.9). We carefully centred the laser focus on the nanodimer and optimized for maximum Raman/SERS signal.[25,26,56,64] The polarization of the incoming light was controlled by a Fresnel rhomb. The polarization of the scattered light was chosen by combining a $\lambda/2$ wave plate to rotate the polarization with an analyser in front of the spectrometer. The elastically scattered laser light was supressed by a notch filter. The inelastically scattered light was analysed with a single stage of a T64,000 spectrometer equipped with a CCD. The laser was tuned in the energy region of the plasmonic and nanotube resonance. To account for the varying sensitivity of the experimental setup, we normalized the Raman spectra to the intensity of CaF_2, which is a standard reference material in Raman spectroscopy. The resonance tuning was performed for the incoming and scattered light polarized along the nanotube axis and the dimer axis. The Raman resonance curve was fit by the expression[52,55]

$$I_R = \left| \frac{\tilde{\mathcal{M}}_{cnt}}{(\omega_i - \omega_{cnt} - \omega_{vib} - i\gamma_{cnt})(\omega_i - \omega_{cnt} - i\gamma_{cnt})} \right|^2, \quad (A1)$$

where $\tilde{\mathcal{M}}_{cnt}$ is the Raman matrix element, ω_{cnt} the resonance energy of the nanotube and γ_{cnt} its width. They were used as fitting parameters. The SERS resonance was fit by Equation (7) using Equation (A1) for the Raman intensity. More details on the experimental conditions and the analysis of the data are given in Wasserroth.[52]